

PAPER • OPEN ACCESS

## Electron scattering cross sections of 1,1,1,2-tetrafluoroethane (R134a)

To cite this article: Marnik Metting van Rijn *et al* 2024 *J. Phys. D: Appl. Phys.* **57** 355202

View the [article online](#) for updates and enhancements.

### You may also like

- [First law and Second law analysis of  \$\text{Al}\_2\text{O}\_3/\text{TiO}\_2\$  nano composite lubricant in domestic refrigerator at different evaporator temperature](#)  
Saravanan K and Vijayan R
- [Performance and energy saving analysis of a refrigerator using hydrocarbon mixture \(HC-R134a\) as working fluid](#)  
M N Mohtar, H Nasution and A A Aziz
- [Influence of  \$\text{Fe}\_2\text{O}\_3\$  and  \$\text{La}\_2\text{O}\_3\$  nanoparticles on the performance of domestic refrigerator functioning with R134a refrigerant](#)  
R Prabu, D Velmurugan, S R Vijayakumar et al.



The Electrochemical Society  
Advancing solid state & electrochemical science & technology

# UNITED THROUGH SCIENCE & TECHNOLOGY

## 248th ECS Meeting

Chicago, IL  
October 12-16, 2025  
*Hilton Chicago*



### Science + Technology + YOU!

Register by  
September 22  
to **save \$\$**

**REGISTER NOW**

# Electron scattering cross sections of 1,1,1,2-tetrafluoroethane (R134a)

Marnik Metting van Rijn<sup>1,\*</sup> , Stephen F Biagi<sup>2</sup> and Christian M Franck<sup>1</sup> 

<sup>1</sup> Institute for Power Systems and High Voltage Technology, ETH Zurich, Zurich, Switzerland

<sup>2</sup> Faculty of Arts and Sciences Physics Department, Uludag University, Bursa, Turkey

E-mail: [marnikm@ethz.ch](mailto:marnikm@ethz.ch)

Received 1 February 2024, revised 18 April 2024

Accepted for publication 23 May 2024

Published 7 June 2024



## Abstract

A revised set of electron-molecule-scattering cross section for the refrigerant R134a ( $\text{CF}_3\text{CH}_2\text{F}$ ) is presented. Swarm studies acquired on a Pulsed Townsend apparatus experimentally verified the electron-transport-coefficient simulations. Increasing the cross sections' quality enhances the accuracy in modelling particle detectors operating with R134a, as the cross sections serve as input for the simulations.

Keywords: pulsed Townsend, cross section, resistive plate chambers, R134a

## 1. Introduction

The refrigerant 1,1,1,2-tetrafluoroethane (see figure 1) is a widely used hydrofluorocarbon commonly known as R134a with applications ranging from automotive air conditioning systems to medical use. Resistive Plate Chambers (RPCs) detect free charged particles in experiments at high-energy physics laboratories. Electrodes confining the chambers generate an electric field, inducing electron avalanches in the gas when free charged particles are present. The standard mixtures used in the RPCs at CERN primarily consist of R134a [1]. Accurately modelling the response of R134a to charged particles in electric and magnetic fields is an important step in the development and improvement of RPC detectors. Simulating the detector's performance requires the electron-molecule-scattering cross sections and enables evaluating novel gas mixtures [2].

R134a cross sections were first derived in 2002 and implemented in MAGBOLTZ7.2. This allowed the drift velocity and effective ionization coefficients to be compared to the measurements of Basile *et al* [3]. The 2002 cross-section set was a

scaled version of the  $\text{C}_2\text{F}_6$  cross-section set used in MAGBOLTZ with an additional cross section covering the CH vibrational excitation at 0.37 eV. The 2002 set gave an accuracy of 5% on the drift velocity and 12% on the effective ionization coefficients in comparison to Basile *et al*.

In 2009, de Urquijo *et al* [4] published measurements of drift velocity, longitudinal diffusion and effective ionization coefficient in both the pure gas and various mixture concentrations with argon. The measurements enabled a more accurate derivation of the vibrational excitations, which was included in the MAGBOLTZ8.91 update in 2010. The new measurements were fitted to better than 5% on drift velocity and 10% on effective ionization coefficient using this new cross-section set. In 2013, Šašić *et al* [5] published a modified cross-section set using the new mixture data of de Urquijo *et al*. The MAGBOLTZ7.2 cross-section set was used as an initial starting point. The omission of the CH vibrational cross section from the starting point, however, caused problems with the subsequent analysis.

In 2023, it was decided to address the difficulties encountered in the previous MAGBOLTZ analysis of R134a. This decision was motivated by the availability of new data on the Computational Chemistry Comparison and Benchmark Data Base (CCCBDB) for the vibrational energy levels and their dipole transition strength [6]. In previous analyses, the vibrational level energies were assumed to be equal to the levels in  $\text{C}_2\text{F}_6$ . Additional data on electron-driven fragmentation [7] and computational calculations [8]

\* Author to whom any correspondence should be addressed.



Original Content from this work may be used under the terms of the [Creative Commons Attribution 4.0 licence](https://creativecommons.org/licenses/by/4.0/). Any further distribution of this work must maintain attribution to the author(s) and the title of the work, journal citation and DOI.

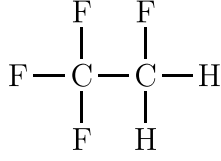


**Figure 1.** Chemical structure of the hydrofluorocarbon 1,1,1,2-tetrafluoroethane (R134a).

were published more recently, complementing the available photoionization studies [9]. New swarm measurements in argon-R134a mixtures spanning the R134a concentration from 0.5% to 2.1% were furthermore performed at ETH Zurich. The additional information impose physical restrictions on the revised set, increasing the weight of evidence in favor of the found cross sections.

The R134a cross sections further serve as the basis for establishing more sophisticated detector simulations. Discrepancy between the simulations and experimental RPC data stemming from the cross sections can thus be mitigated.

## 2. Methods

### 2.1. Pulsed Townsend experiment

The Pulsed Townsend experiment situated at the High Voltage Laboratory at ETH Zurich was described in detail by Haeffiger and Franck [10]. In the meanwhile, the apparatus has undergone only minor changes. A new transimpedance amplifier by FEMTO (HCA-100M-50K-C) with a 100 MHz bandwidth replaced the former FEMTO (HCA-400M-5K-C) for noise reduction. Neutral density filters were mounted to reduce the laser intensity at high electric field strengths, whereas the applied photocathode consists of a nanocrystal layer [11].

The gases used for the measurements were R134a provided by TEGA with a mass purity of 99.5% and argon by ALPHAGAZ with a purity of 99.9999%. The vacuum chamber's base pressure reached  $10^{-7}$  mbar. This base pressure enabled measurements with particle-impurity ratios arising from prior fillings and leakages to stay below 0.1%. The applied reduced electric fields  $E/N$  are reported in the Townsend unit ( $1 \text{ Td} = 1 \times 10^{-21} \text{ Vm}^2$ ), where  $E$  is the electric field and  $N$  the particle density. The pressure is denoted as  $p$ .

Swarm measurements allow the study of macroscopic electron-transport phenomena. Based on the experimental set up and on an appropriate underlying theoretical derivation, specific transport coefficients can be determined as fitting parameters from the acquired signals. Derivations resulting from the Boltzmann transport equation with boundary conditions reveal a concise formula for the induced current in a Pulsed Townsend experiment. The following formula was proposed [12] for the induced current  $I$  as function of time  $t$

$$I(t) = \frac{n_0 e W_F}{2d} \exp(R_{\text{net}} t) \left[ \operatorname{erfc} \left( \frac{W_B t - d}{\sqrt{4D_B t}} \right) - \exp \left( \frac{W_B d}{D_B} \right) \operatorname{erfc} \left( \frac{W_B t + d}{\sqrt{4D_B t}} \right) \right] \quad (1)$$

with  $n_0$  the primary number of emitted electrons with elementary charge  $e$ . The gap distance is  $d$ . The flux drift velocity  $W_F$  is the averaged microscopic drift velocity of the electrons. The total number of charged particles evolves by the rate  $R_{\text{net}}$  [13], which is positive when electric fields exceeding the critical electric field strength are applied. The function  $\operatorname{erfc}$  denotes the complementary error function. The bulk drift velocity  $W_B$  coincides with the center-of-mass velocity of the swarm [13]. Longitudinal bulk diffusion is included via the term  $D_B$ .

Multiple assumptions are, however, required for deriving equation (1), whose validity must be investigated for each measurement. The primary assumption imposes the restriction of the hydrodynamic regime, where the phase-space-density function is developed in an expansion in gradients in the charged-particle density. The resulting continuity equation is then truncated at the third order of the spatial gradient, thereby strictly excluding spatially-asymmetric solutions for the travelling pulse. This assumption's validity is violated when strongly non-conservative processes are present, i.e. in regimes of strong net ionization or strong net attachment. The solution to the continuity equation up to second order is a travelling pulse with a Gaussian envelope [14], which is a spatially-symmetric function.

Skewness in the charged particle density arising from the energy-dependent nature of non-conservative processes are not covered in the solution to second order. The swarm's center of mass defines the bulk-drift velocity and is not influenced by skewness. It is, however, numerically challenging to extract the center of mass. The center of a symmetric Gaussian travelling pulse fitted by regular least-squares method to the skewed shape generally does not coincide with the center of mass. The extracted drift velocity from the Pulsed Townsend experiment thus does not necessarily represent the center-of-mass velocity of the swarm. It is nevertheless reported as  $W_B$ .

An approach to increase the accuracy of the drift-velocity measurements involves measuring at multiple distances and extracting the slope from a linear fit to the distance as function of electron transit time [15]. This certainly reduces the systematics arising from non-equilibrium and boundary effects close to the photocathode [16]. Due to constant-applied reduced electric field  $E/N$ , the conditions are equivalent at the photocathode for varying distance. Boundary effects at the anode may however influence the absorption differently, as the travelling pulse reveals different spatial extend at the arrival for varying distance. Further investigation is required to clarify the significance of this effect, as it contributes to the drift-velocity uncertainty.

Considering contributions up to second order in the electron continuity equation, it was shown that the effective ionization coefficient is given by [17]

$$\alpha_{\text{eff}} = \frac{W_B}{2D_B} - \frac{1}{2D_B} \sqrt{W_B^2 - 4D_B R_{\text{net}}}, \quad (2)$$

which can be deduced from the quantities defined in equation (1).

Extracting the electron-transport coefficients from the induced current measured on a Pulsed Townsend experiment



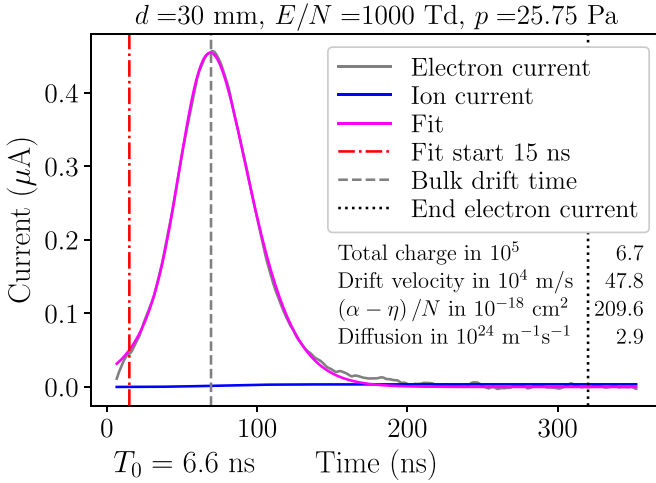


**Figure 2.** Signal acquired on a Pulsed Townsend experiment reveals drift velocity  $W_B$ , the density-reduced effective ionization coefficient  $(\alpha - \eta)/N$ , and the diffusion  $D_B N$ . The factor  $\alpha$  accounts for pure ionization, whereas  $\eta$  represents attachment. The density-reduced effective ionization is calculated using equation (2).

relies on fitting a theoretically-derived equation to the signal (see figure 2). The ion current (blue line) is subtracted from the acquired current in an iterative process [18], where the boundary condition is set such that the electron contribution vanishes for times significantly larger than the electron transit time. This is ensured by either manually setting an ‘End electron current’ (black dotted line) or by solving for a time  $t$  at which the argument in the first erfc function exceeds a certain factor (see equation (1)). The arrival of the laser pulse at the photocathode is denoted as  $T_0$ . Due to initial laser broadening (1.5 ns FWHM) and bandwidth limitations, this value is challenging to determine, and contributes to the inevitable uncertainties at high-electric-field measurements. The influence of ringing and non-equilibrium effects are reduced upon fitting the ion-subtracted electron current (grey curve) only after a certain time ‘Fit start’ (red dashed dotted line). This value is set manually. The vertical grey dashed line denoted as ‘Bulk drift time’ indicates the time at which  $t = L/W_B$ , i.e. when the center of mass is supposed to arrive in absence of diffusion.

Measurements at high electric fields are primarily performed at reduced pressures and small gap distance, ensuring negligible space-charge effect and preventing Townsend discharges. A source capacitance is expected to reduce the transimpedance amplifier’s bandwidth severely. A prior estimate for the amplifier’s bandwidth was reported at 36 MHz for the current apparatus [10], which results in a rise time of around 10 ns. The upgraded amplifier is not expected to alter the bandwidth.

The uncertainty on the reported transport coefficients are expected to be 10% on the drift velocity  $W_B$ , 20% on the effective ionization coefficient  $\alpha_{\text{eff}}$ , and 20% on the longitudinal diffusion  $D_B$ . The dominant two contributions to the uncertainty in the drift-velocity measurements can be assigned to bandwidth limitations and an initial thermalization process. Bandwidth limitations induce rise times of around 10 ns,

which lead to 5% uncertainty in the drift velocity measurements for 100 ns drift times. An initial thermalization process occurring upon electron injection into the gas has shown to alter the drift velocities by an additional 5%, thereby justifying the overall estimate of 10% uncertainty. Extracting accurate longitudinal diffusion values is challenging, as it is determined during the absorption process and thus severely influenced by boundary effects. Initial broadening from the laser is not taken into account while applying equation (1). The uncertainty in the effective ionization coefficient is related to the longitudinal diffusion coefficient (see equation (2)).

## 2.2. Simulations

Various approaches in modelling the electron motion in a gas with applied electric field exist [19–21]. Approximate Boltzmann-transport-equation solvers often truncate the expansion of the electron density distribution function in spherical harmonics at the second order, which is known as the two-term approximation. This simplification significantly reduces the computing time, but may result in inaccurate transport values [22].

Monte–Carlo simulations yield reliable results [23, 24], while the accuracy is only limited by computing time. The Monte–Carlo solver MAGBOLTZ calculates the drift velocities, diffusion coefficients and the effective ionization coefficients for a large number of gases to high accuracy. The simulations can be experimentally verified using swarm measurements, which are typically dependent on the cross sections up to around 30 eV incident electron energy.

The Monte–Carlo simulation MAGBOLTZ was described in detail in [23], whereas certain modifications were done thereafter. The approach of Okhrimovskyy *et al* [25] was implemented to cover anisotropic elastic scattering. Based on the first Born approximation, the differential cross section of the screened Coulomb potential is extended with a fitting parameter [26], which can be deduced from the ratio between the momentum-transfer and the total cross section. This method is very accurate as it is exact up to the first moment of the angular distribution. For electric field strengths above 1000 Td, the first moment typically only influences the drift velocities by 1% to 3%. Higher moments can thus often be neglected.

The calculated electron drift velocities are specified by their theoretical interpretation following the notation of Satoh *et al* [16], where the center-of-mass velocity is denoted as  $W_r$ . This quantity corresponds to the bulk drift velocity  $W_B$  in the notation of Casey *et al* [12] (see equation (1)). The average electron drift velocity  $W_v$  coincides with the flux drift velocity  $W_F$ . The mean-arrival-time drift velocity  $W_M$  results from time-of-flight experiments.

The cross sections at higher energies determine the asymptotic  $W$ -value, which is the average energy required for generating an electron-ion pair. The program DEGRAD can calculate the  $W$ -value and Fano factors, giving consistency for the cross sections above 30 eV. Fano factors determine the energy resolution of gaseous particle detectors. The factors relate the

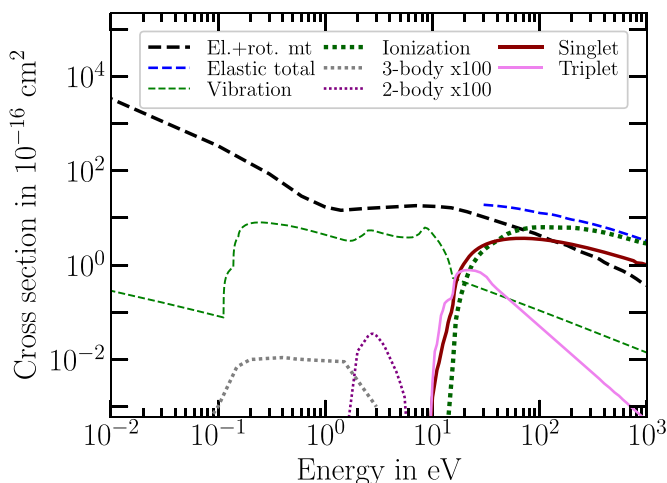


**Figure 3.** Cross section of R134a. Ionization accounts for gross ionization. The elastic and rotational momentum-transfer cross sections are summed and represented as El.+rot. mt.

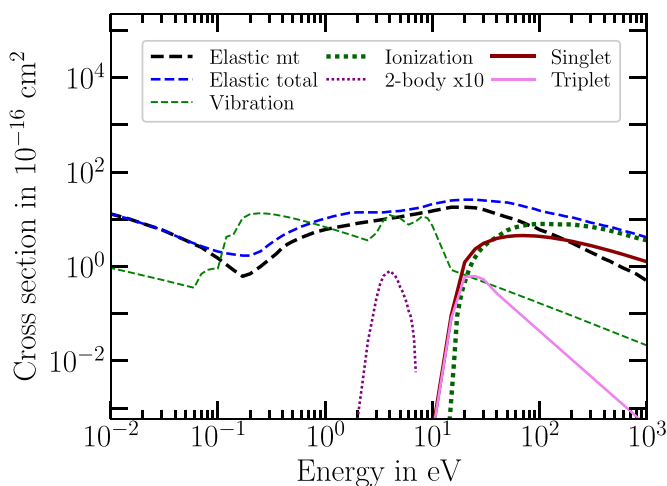


**Figure 4.**  $C_2F_6$  cross section taken from MAGBOLTZ.

variability of the generated amount of charge with the incident particle's energy.

In this work, calculations were undertaken to computational accuracies of 0.1% on the drift velocity, 4% on the diffusion and 3% on the effective ionization coefficient.

### 3. Results

#### 3.1. $C_2H_2F_4$ cross section set

The derived cross sections in the analysis were forced to follow experimental and theoretical constraints, and to exhibit smooth behavior with energy (see figure 3). R134a is expected to have comparable cross sections as  $C_2F_6$ , as both gases reveal similar structure. The  $C_2F_6$  cross sections (see figure 4) are used extensively when deriving the R134a cross sections.

The elastic cross section in hydrofluorocarbons can be combined with the rotational excitation cross sections. The energy spacings of the rotational levels are close to the kinetic energy

**Table 1.** Vibrational excitation levels in R134a.

Energy in eV	Association
0.1125	CF bend
0.139	CF stretch
0.155	CF stretch
0.374	CH stretch
0.5	Higher harmonics

loss encountered by an electron in elastic collisions, justifying the combination of the two cross sections. The average energy loss to rotation and elastic scattering is typically less than 1 meV in R134a. This is in contrast to hydrocarbons where the rotational energy spacing are typically exceeding 5 meV. The difference lies in the moments of inertia of hydrocarbons, which are a factor of 10 smaller.

The R134a molecule reveals a static dipole moment of 1.9 D [27], slightly exceeding that found in  $H_2O$  (1.86 D [28]). The dipole moment contributes to the summed elastic and rotational cross section at low energy, where it decreases with energy as  $1/E$  (see figure 3). The enhanced dipole moment further obscures the Ramsauer minimum, thereby giving a similar shape in summed elastic and rotational cross section as found in  $H_2O$  [29]. In contrast, the summed elastic cross section in  $C_2F_6$  exhibits a more pronounced Ramsauer minimum at around 170 meV and a reduced elastic cross section at low energies due to zero dipole moment (see figure 4).

Hydrofluorocarbons have large dipole transition moments in comparison to hydrocarbons. The enhanced transition moments can be explained by the polar nature of the CF bonds in comparison to the non-polar CH bonds. The transition energies and moments were taken from CCCBDB provided by NIST [6]. The method of grouping close transitions together was followed, which allowed the separation of the energies into 5 effective vibrational levels at energies of 0.1125 eV, 0.139 eV, 0.155 eV, 0.374 eV and 0.5 eV. These levels correspond to CF bend, CF stretch, CF stretch, CH stretch, and to the sum of higher harmonics (see table 1). The two effective CF stretch vibrations have the dominant transition strengths, but all vibrational excitations contribute to the transport calculations.

The vibrational shape function is assumed to be a standard born dipole with resonance enhancements at higher energy. The resonance enhancements in the previous analysis, MAGBOLTZ8.9I, were assumed to be at the same energy as in  $C_2F_6$ . The new analysis allowed the lower resonance peak to vary in energy. The best fit was obtained upon moving the lower peak in energy to 2.8 eV.

The superelastic vibrational transition cross-sections are derived from the vibrational cross-sections by the Klein Rossland detailed balance equation [30]. The calculated vibrational level populations were deduced from the given gas temperature.

The electronic excitation energy levels were split into dipole-allowed and non-dipole transitions from the ground state. The data available such as photoabsorption in R134a was not of sufficient accuracy or range to be included in the

analysis. Therefore, a copy of the  $C_2F_6$  cross-section set from MAGBOLTZ was used. The threshold energy of each level was reduced by 0.5 eV and scaled by 0.76 in amplitude. The factor 0.76 is the ratio of total number of electrons in R134a in comparison to  $C_2F_6$ .

The dipole allowed levels were at 9.4 eV, 10.4 eV, 11.8 eV, 13.4 eV, 15.4 eV and 20.4 eV with oscillator strengths of 0.011 97, 0.020 18, 0.094 39, 0.3523, 3.892 and 1.943 respectively. The oscillator strengths are adapted from the  $C_2F_6$  cross sections [31]. The shape of the dipole allowed transitions was defined by the BEF scaling law [32].

The triplet levels were set at 9.3 eV, 10.3 eV, 11.7 eV and 14.7 eV. The shape of the triplet cross-sections as a function of energy followed the standard linear rise followed by a  $1/E^2$  fall off from a peak at twice the level energy. In the transport calculation only the amplitude of the triplet levels was allowed to vary in order to fit the effective ionization coefficient measurements.

The attachment cross-section in R134a contains both a two-body-dissociative and a three-body component. The peak of the first vibrational resonance in both  $C_2F_6$  and  $C_3F_8$  are at the energy of the two-body attachment cross-section in both these molecules. Since there are no attachment-cross-section measurements conducted with electron scattering, the same mechanism of two-body attachment in R134a is assumed. A two-body-peak cross section at the first vibrational resonance in R134a at 2.8 eV is thus expected.

$C_2F_6$  does not reveal three-body attachment, whereas  $C_3F_8$  does. The three-body attachment in R134a, however, is not of a similar nature to the three-body attachment in  $C_3F_8$ . The three-body-attachment cross section in R134a was derived manually such that it fits to the pressure dependent measurements of Basile *et al.* The most likely explanation of the broad shape of the three-body attachment cross section is that it is due to attachment to dimers. The dimers in R134a are easily formed by the attraction of the large dipole moment 1.9 D of the molecule. A similar situation exists in water where large clusters are observed, causing three-body attachment. Both three-body and two-body attachment are well fitted by the cross-sections used in the analysis. The attachment rates are very small and do not affect the other transport parameters and can be analyzed independently of the other cross-sections.

There is no useful experimental ionization cross-sections published to date for R134a. An improvement since the last update in 2010 is that the threshold energy for ionization has been measured [7]. The experimentally found value is 13.2 eV. The previous MAGBOLTZ analyses used a value of 14.48 eV for the ionization, which is 1.2 eV larger and introduced some errors in the previous analyses. The new ionization energy is in better agreement with the  $C_2F_6$  ionization energy, which is 13.7 eV. The lower energy for R134a is expected from the systematic behavior of hydrofluorocarbons.

Experimental data on dissociative and non-dissociative ionization in R134a is limited. The  $C_2F_6$  gross-ionization cross section is, however, well measured. The R134a gross-ionization is thus taken from  $C_2F_6$  and shifted lower in energy by 0.5 eV and scaled in amplitude by 0.76. This procedure

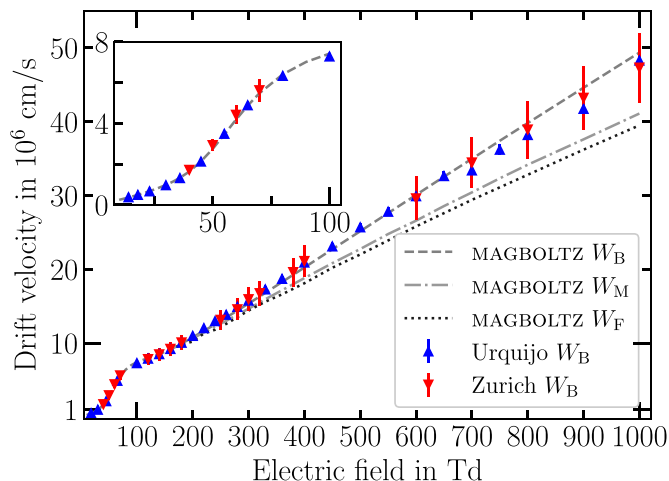


**Figure 5.** Electron drift velocity in pure R134a compared to simulations based on the revised R134a cross sections. A constant diffusion was assumed above 800 Td in order to calculate de Urquijo's bulk drift velocity at 900 Td and 1000 Td.

should yield the gross-ionization cross sections that are accurate to better than 10%. The value of the ionization cross section was kept constant in the fitting procedure to the experimental effective ionization coefficient and only the triplet excitation scattering was varied.

### 3.2. Experimental validation

The measured electron bulk drift velocities  $W_B$  in pure R134a were compared to the MAGBOLTZ simulation of the revised cross-section set (see figure 5). The measurements were taken at pressures varying between 25 Pa and 2000 Pa, depending on the generated number of charges, which was limited to around  $10^6$ , ensuring negligible space-charge effects. Solving the Poisson equation of the electron and ion charge densities in the avalanche and comparing the associated electric field with the applied electric field predicts the significance of space-charge effects [33]. Estimates were applied to the Pulsed Townsend experiment resulting in a threshold of  $10^6$ , below which space charge has no significance influence. The cross sections were fitted to the measurements of de Urquijo *et al* where the deviations are shown in figure 6.

The pronounced Ramsauer minimum, and the absence of rotational and vibrational excitations in argon result in a high sensitivity to perturbations in the low-energy regime. Adding small amounts of a different gas with significant elastic cross sections and excitations in the lower energy regime thus decisively alters the electron-transport coefficients. Argon-diluted R134a mixtures were measured at 40 kPa to verify the elastic and vibrational excitation cross sections in R134a (see figure 7). The simulations were performed using MAGBOLTZ with the argon cross sections defined therein. The deviations in the drift velocity are shown as a function of mean energy in figure 8.

The corresponding R134a diffusion measurements were performed in argon-diluted mixtures (see figure 9), where

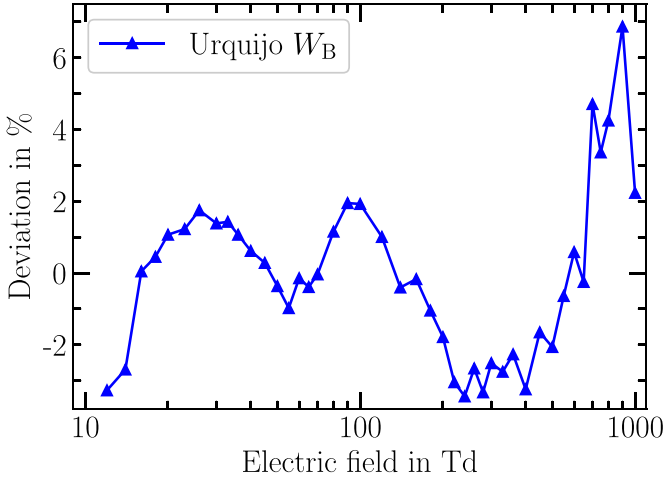


**Figure 6.** Deviation between the simulation of  $W_B$  and de Urquijo's data.

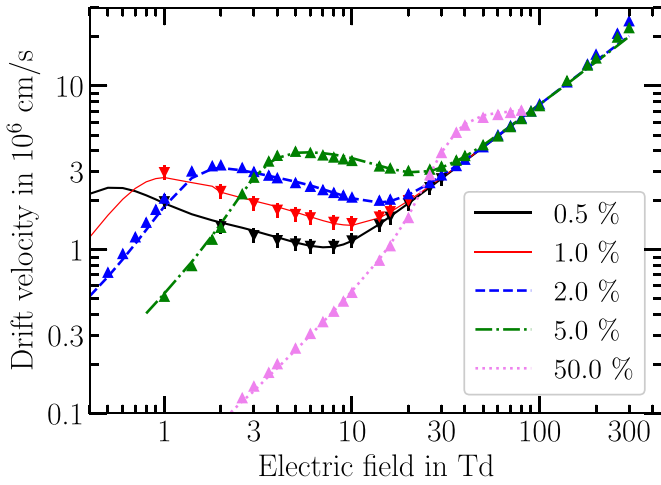


**Figure 7.** Drift velocity  $W_B$  in argon-diluted R134a mixtures, where percentage represents the R134a concentration. The continuous lines are the MAGBOLTZ simulations for the measurements acquired in Zurich. The non-continuous lines are MAGBOLTZ simulations for the data provided by de Urquijo *et al* where the errorbars are within the markers.

the deviations are shown as a function of mean energy (see figure 10). The measurements range from 1 Td to 30 Td and were taken at a pressure of 40 kPa.

The effective ionization coefficient measured by de Urquijo *et al* are compared to the cross section simulations (see figure 11). Based on equation (1), the acquired signal provides the effective ionization rate  $R_{\text{net}}$ . Translating this coefficient into a spatial effective ionization coefficient  $\alpha_{\text{eff}}$  was done according to equation (2). The data points presented are from the same measurements shown in figure 5.

The  $W$ -value was calculated using DEGRAD over 6 orders of magnitude in energy (see figure 12). The asymptotic  $W$ -value was found at 30.7 eV/ion pair.

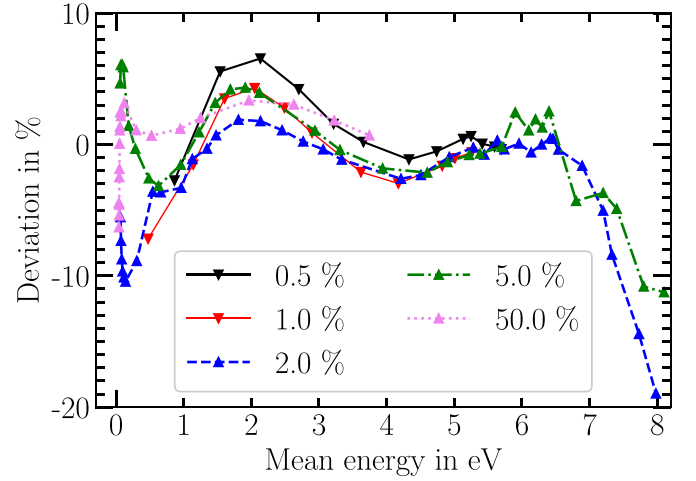


**Figure 8.** Deviation between simulations and measured drift velocities in argon-diluted mixtures. The connecting lines serve as a guide to the eye. The continuous lines refer to measurements acquired in Zurich. The dashed lines are from de Urquijo *et al*.

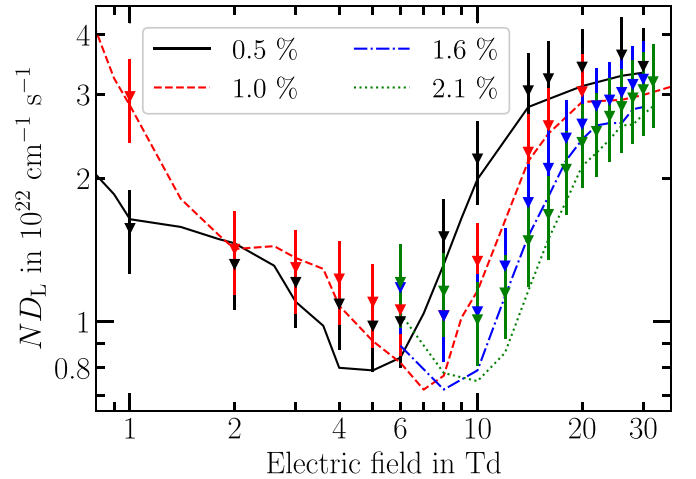


**Figure 9.** Diffusion in argon-diluted R134a mixtures, where percentage represents the R134a concentration. All measurements acquired in Zurich.

#### 4. Discussion

The Pulsed Townsend experiment requires delicate care for measurements up to 1000 Td in reduced electric field. The underlying assumption based on a longitudinally, symmetrically-broadening Gaussian spatial electron distribution is perturbed in shear and kurtosis. Extracting and associating the drift velocities to theoretically-derived quantities remains challenging when boundary effects and bandwidth limitations are present.

The experimental data of de Urquijo *et al* for argon mixing ratios greater than 2% and the Zurich data for less than 2% were included in the fitting. The experimental drift velocity in the mixtures was fitted by varying the amplitude of the vibrational cross sections until a close fit was achieved. The

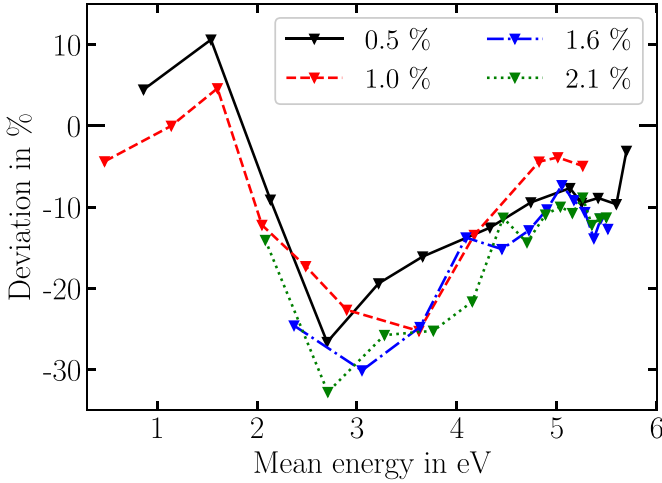


**Figure 10.** Deviation between simulations and measured diffusion coefficients in argon-diluted mixtures. The connecting lines serve as a guide to the eye. All measurements acquired in Zurich.

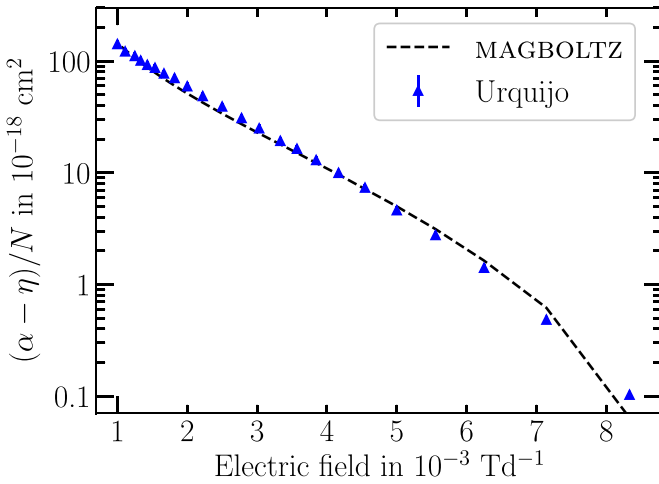


**Figure 11.** Effective ionization coefficient in pure R134a shown as a function of inverse reduced electric field strength.

drift velocity in the pure gas was then used to give a good fit for the elastic cross section. This process was repeated a few times until the fit to the drift velocities was within experimental error.

During this process it became clear that the position of the first resonance in the vibrational cross section needed to be reduced in energy. The resulting energy shift in the position of the first vibrational resonance reduced the average drift velocity deviations in the argon mixtures to 7% at swarm energies close to 2 eV (see figure 8). The final fit to the pure gas drift velocity is shown in figure 5 and the deviations are within an average of 2% except for the electric field strengths exceeding 700 Td (see figure 6). The prior R134a cross section set revealed a deviation of 5% on the pure drift velocity.

The ionization and attachment cross sections were fit to the data of Basile *et al* and de Urquijo *et al*. The fit involved only varying the amplitude of the triplet excitation cross sections

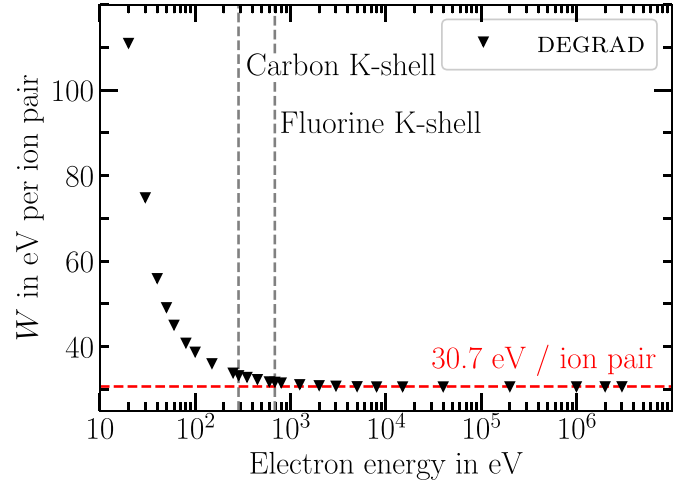


**Figure 12.**  $W$ -values in R134a simulated by DEGRAD. The red, dashed line corresponds to the asymptotic value at high energies.

until the best agreement with data was achieved. The dipole allowed excitations and ionization cross-section were fixed in the fit. The agreement between experiment and data is generally within 12%. The experimental data are quoted as having an error of 10%, which may be an underestimate. No further attempt was made to improve the fitting to the ionization coefficient since accurate experimental data on the dissociative ionization cross sections and the oscillator strengths of the excitations are not available.

The large experimental errors on the longitudinal diffusion of 20% (see figure 10) did not allow any constraints on the cross sections. Within the experimental errors, the calculated diffusion is consistent with the experimental data except at mean swarm energies around 3 eV.

A cross check of the consistency of the cross section set for the ionization and excitation at energies above 30 eV is the  $W$ -value. This value describes the mean average energy required to generate an ion pair upon irradiating the gas with charged particles or x-rays. The value of  $W$  for the hydrofluorocarbons is normally between 30 eV–34 eV per ion pair. In contrast, the hydrocarbons, which are more weakly bound, have  $W$ -values between 22 eV–26 eV. The  $W$ -value in the literature is normally taken to be the asymptotic value at energies above 2 keV.

The calculation using DEGRAD for R134a for a range of energies gives a  $W$ -value of 30.7 eV for the asymptote (see figure 12). This value is in a similar range with the other hydrofluorocarbons. The  $W$ -value is most sensitive to the ratio of the ionization to excitation cross section above 30 eV and gives confidence in the accuracy of the extracted cross-section set.

## 5. Conclusion

This work was undertaken to enable more accurate modelling of the response of RPC radiation detectors, which use mixtures containing R134a. These detectors operate at high electric fields above 200 Td with swarm energies ranging between



4 eV–7 eV. The extracted cross-section set is most accurate at energies above 1 eV and therefore is of good accuracy for simulating RPC-detector responses.

The improvements in the vibrational energy thresholds and also position of the first vibrational resonance combined with a more accurate ionization energy threshold, and the splitting of the excitation into dipole-allowed and triplet levels give an improved fit to the electron-transport data. The cross sections are consistent with the scaled  $C_2F_6$  cross sections, which are well measured.

The reduced spread of the deviations from the experimental transport data obtained here should give the calculated drift velocity in these RPC mixtures to better than 7% and the effective ionization coefficient to better than 10%.

## Data availability statement

The data that support the findings of this study will be openly available following an embargo on LxCat [34] under the following URL/DOI: [www.lxcat.net/ETHZ](http://www.lxcat.net/ETHZ). Data will be available from 1 January 2025.

## Acknowledgment

This work was supported by the Swiss NSF under Grant No. 200021\_212060 for the project entitled ‘Environmental Friendly Gas Mixtures for Gaseous Tracking and Timing Detectors’.

## ORCID iDs

Marnik Metting van Rijn  <https://orcid.org/0009-0006-1259-4952>

Christian M Franck  <https://orcid.org/0000-0002-2201-7327>

## References

- [1] Rigoletti G *et al* 2020 Studies of RPC detector operation with eco-friendly gas mixtures under irradiation at the CERN Gamma Irradiation Facility *Proc. Sci.* **364** 164
- [2] Veenhof R 1998 Garfield, recent developments *Nucl. Instrum. Methods Phys. Res. A* **419** 726–30
- [3] Basile G, Gallimberti I, Stangherlin S and Teich T H 1991 XX *Int. Conf. on Phenomena in Ionized Gases 2* (9 July 1991)
- [4] de Urquijo J, Juárez A, Basurto E and Hernández-Ávila J 2009 Electron swarm coefficients in 1,1,1,2-tetrafluoroethane (R134a) and its mixtures with Ar *Eur. Phys. J. D* **51** 241–6
- [5] Šašić O, Dupljanin S, de Urquijo J and Petrović Z L 2013 Scattering cross sections for electrons in  $C_2H_2F_4$  and its mixtures with Ar from measured transport coefficients *J. Phys. D: Appl. Phys.* **46** 325201
- [6] Johnson R D III 1999 NIST 101. Computational chemistry comparison and benchmark database (Computational Chemistry Comparison and Benchmark Database) (available at: <http://cccbdb.nist.gov>)
- [7] Pereira-da Silva J *et al* 2021 Electron driven reactions in tetrafluoroethane: positive and negative ion formation *J. Am. Soc. Mass Spectrom.* **32** 1459–68
- [8] Hayashi T, Ishikawa K, Sekine M and Hori M 2018 Dissociative properties of 1,1,1,2-tetrafluoroethane obtained by computational chemistry *Jpn. J. Appl. Phys.* **57** 06JC02
- [9] Zhou W, Seccombe D P and Tuckett R P 2002 Fragmentation of valence electronic states of  $CF_3-CH_2F^+$  and  $CHF_2-CHF_2^+$  in the range 12–25 eV *Phys. Chem. Chem. Phys.* **4** 4623–33
- [10] Haeffliger P and Franck C 2018 Detailed precision and accuracy analysis of swarm parameters from a pulsed Townsend experiment *Rev. Sci. Instrum.* **89** 023114
- [11] Yarema O *et al* 2023 Palladium zinc nanocrystals: nanoscale amalgamation enables multifunctional intermetallic colloids *Adv. Funct. Mater.* **2309018**
- [12] Casey M, Stokes P, Cocks D G, Bošnjaković D, Simonović I, Brunger M J, Dujko S, Petrović Z L, Robson R E and White R 2021 Foundations and interpretations of the pulsed-Townsend experiment *Plasma Sources Sci. Technol.* **30** 035017
- [13] Tagashira H 1987 Principles of the measurement of electron drift velocities *Swarm Studies and Inelastic Electron-Molecule Collisions: Proc. Meeting 4th Int. Swarm Seminar and the Inelastic Electron-Molecule Collisions Symp. (Tahoe City, California, USA, 19–23 July 1985)* (Springer) pp 55–61
- [14] Huxley L G H and Crompton R W 1974 Diffusion and drift of electrons in gases (Wiley)
- [15] Vass M, Egüz E, Chachereau A, Hartmann P, Korolov I, Hösl A, Bošnjaković D, Dujko S, Donko Z and Franck C M 2020 Electron transport parameters in  $CO_2$ : a comparison of two experimental systems and measured data *J. Phys. D: Appl. Phys.* **54** 035202
- [16] Satoh K, Ohmori Y, Sakai Y and Tagashira H 1991 Computer simulation study of correspondence between experimental and theoretical electron drift velocities in  $CH_4$  gas *J. Phys. D: Appl. Phys.* **24** 1354
- [17] Tagashira H, Sakai Y and Sakamoto S 1977 The development of electron avalanches in argon at high E/N values. II. Boltzmann equation analysis *J. Phys. D: Appl. Phys.* **10** 1051
- [18] Chachereau A 2018 Electron and ion kinetics in fluorinated gases for electrical insulation *PhD Dissertation* ETH Zurich
- [19] Hagelaar G and Pitchford L C 2005 Solving the Boltzmann equation to obtain electron transport coefficients and rate coefficients for fluid models *Plasma Sources Sci. Technol.* **14** 722
- [20] Biagi S 1989 A multiterm Boltzmann analysis of drift velocity, diffusion, gain and magnetic-field effects in argon-methane-water-vapour mixtures *Nucl. Instrum. Methods Phys. Res. A* **283** 716–22
- [21] Boyle G, Tattersall W, Cocks D, McEachran R and White R 2017 A multi-term solution of the space-time Boltzmann equation for electrons in gases and liquids *Plasma Sources Sci. Technol.* **26** 024007
- [22] White R D, Robson R E, Schmidt B and Morrison M A 2003 Is the classical two-term approximation of electron kinetic theory satisfactory for swarms and plasmas? *J. Phys. D: Appl. Phys.* **36** 3125
- [23] Biagi S 1999 Monte Carlo simulation of electron drift and diffusion in counting gases under the influence of electric and magnetic fields *Nucl. Instrum. Methods Phys. Res. A* **421** 234–40
- [24] Rabie M and Franck C M 2016 METHES: a Monte Carlo collision code for the simulation of electron transport in low temperature plasmas *Comput. Phys. Commun.* **203** 268–77
- [25] Okhrimovskyy A, Bogaerts A and Gijbels R 2002 Electron anisotropic scattering in gases: a formula for Monte Carlo simulations *Phys. Rev. E* **65** 037402

- [26] Belenguer P and Pitchford L 1999 Effect of anisotropy in the elastic scattering cross sections on the ionization source terms in glow discharges in argon *J. Appl. Phys.* **86** 4780–5
- [27] Barao T, de Castro C A N, Mardolcar U V, Okambawa R and St-Arnaud J M 1995 Dielectric constant, dielectric virial coefficients and dipole moments of 1,1,1,2-tetrafluoroethane *J. Chem. Eng. Data* **40** 1242–8
- [28] Shostak S L, Ebenstein W L and Muentner J S 1991 The dipole moment of water. I. Dipole moments and hyperfine properties of H<sub>2</sub>O and HDO in the ground and excited vibrational states *J. Chem. Phys.* **94** 5875–82
- [29] Itikawa Y and Mason N 2005 Cross sections for electron collisions with water molecules *J. Phys. Chem. Ref. Data* **34** 1–22
- [30] Fujimoto T 2008 Plasma spectroscopy *Plasma Polarization Spectroscopy* (Springer) pp 29–49
- [31] Lee L, Phillips E and Judge D 1977 Photoabsorption cross sections of CH<sub>4</sub>, CF<sub>4</sub>, CF<sub>3</sub>Cl, SF<sub>6</sub> and C<sub>2</sub>F<sub>6</sub> from 175 to 770 Å *J. Chem. Phys.* **67** 1237–46
- [32] Kim Y-K 2001 Scaling of plane-wave Born cross sections for electron-impact excitation of neutral atoms *Phys. Rev. A* **64** 032713
- [33] Färber R and Franck C M 2021 Streamer inception thresholds derived from a statistical electron transport model *J. Phys. D: Appl. Phys.* **54** 435202
- [34] Pitchford L C *et al* 2017 LXCat: an open-access, web-based platform for data needed for modeling low temperature plasmas *Plasma Process. Polym.* **14** 1600098